Journal of
Water & Climate Change

IWA PUBLISHING

Journal of Water and Climate Change Vol 14 No 2, 454 doi: 10.2166/wcc.2023.323

Modified version of the cross-correlation function to measure drought occurrence time-delay correlation

Mohammad Reza Mahmoudi[a] and Abdol Rassoul Zarei[b,*]

[a] Department of Statistics, Faculty of Science, Fasa University, Fasa, Fars, Iran
[b] Department of Range and Watershed Management (Nature Engineering), Faculty of Agriculture, Fasa University, Fasa, Iran
*Corresponding author. E-mail: ar_zareiee@fasau.ac.ir; ar_zareiee@yahoo.com

ARZ, 0000-0002-2735-0778

ABSTRACT

According to the importance of assessing the presence of time delay between the occurrence of various hydrological and meteorological phenomena, the study aim is to introduce a new method (with high ability and non-sensitivity to the abnormality of datasets and the existence of outliers) for determining the time delay in mentioned data series. In this research, a new measure to detect the time delay between two stationary time series (Non-Parametric Cross-Correlation Function or NCCF, called Spearman's CCF or SCCF) is introduced, which has very low sensitivity to abnormality of data series and also the existence of outliers in the data series. The numerical studies verify the ability of the proposed measure. In standard uniform and exponential (with mean 1) time series, at 100% of numerical analyses and in standard Gaussian time series at more than 60% of numerical studies, the ability of SCCF was more than the CCF. The applicability of the proposed measure in practice was also studied using the Reconnaissance Drought Index (RDI) data series of 20 stations over Iran during 1967–2019 in 1, 3, and 12-month time scales. The results of the practical study also proved the appropriate performance of the proposed model in all time scales.

Key words: cross-correlation, drought, non-parametric, stationary, time-delay, time series

HIGHLIGHTS

- A modified version of the cross-correlation function was presented.
- Output of this research is a new measure to detect the time delay between two stationary time series.
- In this research, data series of 20 stations with various climate conditions was used.
- The results are usable in better understanding the behavior of climatic parameters (especially drought).

GRAPHICAL ABSTRACT

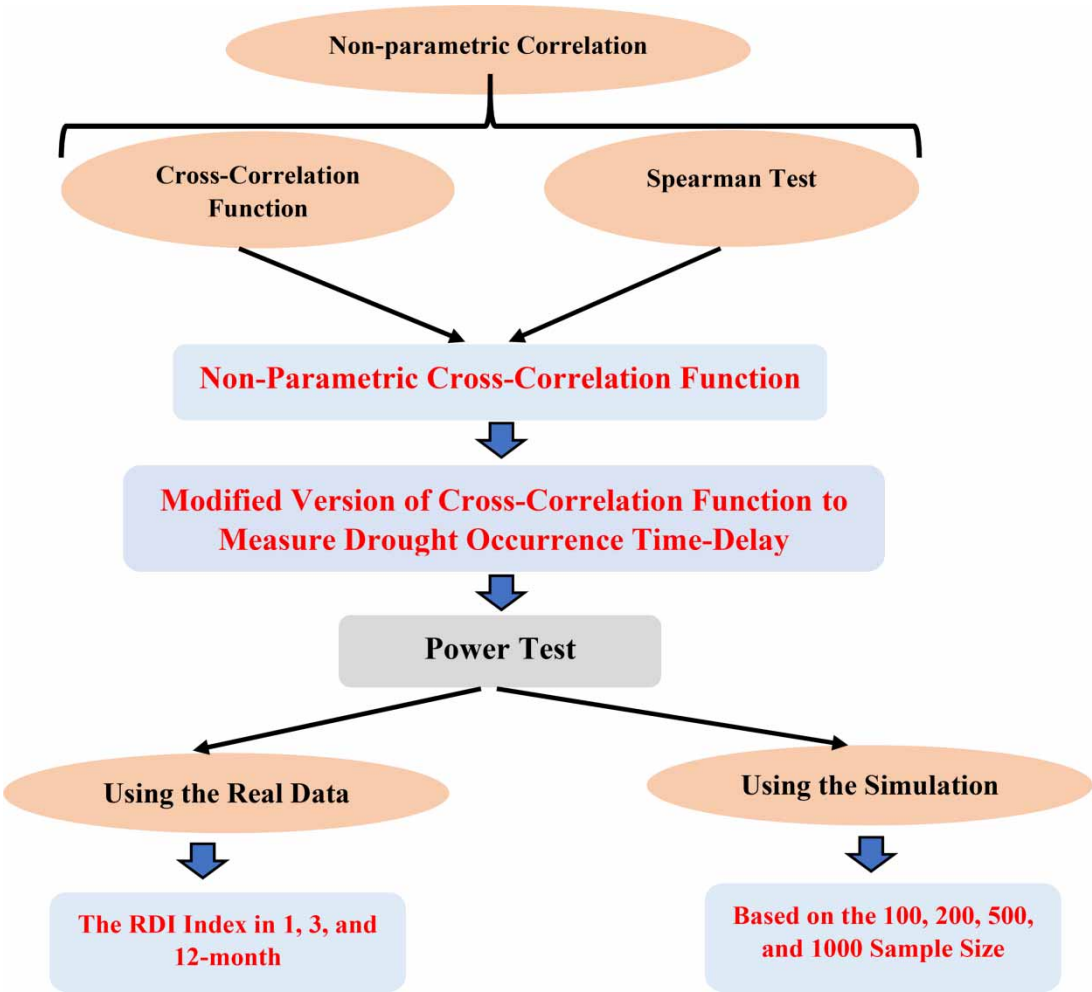

1. INTRODUCTION

The existence of a relationship between different climatic variables and various hydrological phenomena in terms of temporal and spatial is a proven issue worldwide (Abeysingha *et al.* 2020; Aksoy *et al.* 2021; Liang *et al.* 2021; Liu *et al.* 2021; Mokarram & Zarei 2021; Salimi *et al.* 2021; Zarei & Mahmoudi 2021; Zarei *et al.* 2021a; Lotfirad *et al.* 2022; Radmanesh *et al.* 2022; Sun *et al.* 2022). Generally, this relationship is used by researchers in various studies such as assessing and determining the degree of dependence of different variables, examining changes in one variable under the influence of other variables, evaluating the temporal and spatial changes in variables, examining and determining the delay time of a variable in different regions, etc. (Chen *et al.* 2018; Zarei & Moghimi 2019; Zarei *et al.* 2020; Bahrami *et al.* 2021; Fang *et al.* 2021; Gumus *et al.* 2021; Han *et al.* 2021). Therefore, it can be concluded that the detection of relationships between variables has a vital role in meteorological, hydrological, environmental, and so on, studies.

There are several parametric and non-parametric techniques introduced for detecting the relationships such as Pearson's correlation coefficient (Ablat *et al.* 2019; Li *et al.* 2020), Spearman's correlation coefficient (SCCF; Konapala *et al.* 2020; Tai *et al.* 2020), Kendall's correlation coefficient (Peña-Gallardo *et al.* 2019; Mallick *et al.* 2021), the Sen's slope (Atif *et al.* 2018; Myronidis *et al.* 2018), the cross-correlation function (CCF; Seo *et al.* 2019; Dong *et al.* 2020), and so on. Aryal & Zhu (2021) assessed the spatiotemporal structure of drought using the standardized precipitation evapotranspiration index (SPEI) and the principal component analysis over the continental United States during 1950–2015 in 12 and 24-month time scales. The results indicated that the areas with severe drought conditions are mostly located in the Northwest, South, upper

Midwest, and East regions. Zarei *et al.* (2021b) used the CCF to assess the susceptibility of winter wheat, barley, and rapeseed to drought using the meteorological data series of 10 stations during 1968–2017 over Iran. They showed that the rapeseed had been the most susceptibility to drought occurrence. This study indicated that the maximum CC between the drought and annual yield of mentioned crops was less than 0.5 in more than 80% of investigated stations (without time lag). Rahmani & Fattahi (2021) used the multifractal cross-correlation to evaluate the sensitivity of meteorological and hydrological drought to temperature and rainfall. Based on the results of this research, the effect of precipitation fluctuations on droughts was more than the temperature fluctuations. Roustaei *et al.* (2021) assessed the time delay between wind erosion and drought in the Southern regions of Iran using the CCF function. They revealed that the maximum CC between the drought and wind erosion was equal to −0.22 (without time lag). Many researchers have tried to use parametric and non-parametric techniques to detect relationships between climatic and hydrologic variables worldwide (e.g., Baik *et al.* 2021; Kumar *et al.* 2021; Lashkari *et al.* 2021; Lohpaisankrit & Techamahasaranont 2021; Piri & Mobaraki 2021; Tuan & Canh 2021; Zarei *et al.* 2021c; Zhang *et al.* 2021).

Pearson's correlation coefficient is sensitive to the abnormality of datasets and the existence of outliers. Moreover, Pearson's correlation coefficient, Spearman's correlation coefficient, and Kendall's correlation coefficient are more applicable in facing independent observations. For assessing the relationship of two time series, the cross-correlation function (CCF, in abbreviation) is suggested. The CCF is somewhat sensitive to the abnormality of datasets and the existence of outliers (similar to Pearson's correlation). In other words, for abnormal populations or for populations with outliers data, the CCF may not work well. To solve this issue, in this research, we define a non-parametric CCF (NCCF, in abbreviation), called Spearman's CCF (SCCF, in abbreviation). The ability of the SCCF to detect a time-delay correlation between two stationary time series is studied. For this purpose, numerous datasets from two stationary time series are produced and analyzed. The ability of SCCF in practice is also investigated by a real example. For this purpose, the annual reconnaissance drought index (RDI) values from three Iranian synoptic are considered and analyzed.

In other words, due to the vital role of determining the delay time of the hydrological phenomena occurrence (such as drought, rain, and flood) in managing and reducing the negative impacts of the phenomena mentioned above, in this study, a new non-parametric statistical test (NCCF) was presented for determining the delay time in hydrological phenomena (It is the most critical aspect of research novelty). Then, its ability was assessed based on the simulated and real data.

2. MATERIALS AND METHODS

In this section, first, the parametric and non-parametric correlation methods will be explained. Then, the CCF model and its application in determining the time delay in hydrological phenomena will be described. Then, the SCCF model, as a new model for determining the time delay in hydrological phenomena, will be explained. Finally, using simulated data and actual data (based on the RDI drought index in different time scales), the ability of the SCCF model will be investigated.

2.1. Parametric correlation

Assume $(X_1, Y_1), \ldots, (X_n, Y_n)$ is a sample of size n from bivariate population (X, Y). Pearson's correlation coefficient, which is a parametric tool, is more powerful in facing the bivariate normal datasets and is defined as follows (Equation (1)):

$$r = \frac{\sum_{i=1}^{n} (X_i - \bar{X})(Y_i - \bar{Y})}{\sqrt{\sum_{i=1}^{n} (X_i - \bar{X})^2} \sqrt{\sum_{i=1}^{n} (Y_i - \bar{Y})^2}} \tag{1}$$

where X_i and Y_i are the values of the X and Y variables, and $\bar{X}$ and $\bar{Y}$ are the averages of the X and Y variables in the sample.

2.2. Non-parametric correlation

For abnormal datasets or datasets with outliers, the non-parametric tools such as Spearman's correlation coefficient, Kendall's correlation coefficient, and Sen's slope are more robust. To compute SCCF, at first, $X_1, \ldots, X_n$ and $Y_1, \ldots, Y_n$ are separately sorted from smallest to largest. Then, Spearman's correlation is defined as the Pearson's correlation coefficient

of (Equations (2)–(4)).

$$(R_1, S_1), \ \ldots, \ (R_n, S_n) \tag{2}$$

where

$$R_i = rank(X_i) \tag{3}$$

and

$$S_i = rank(Y_i) \tag{4}$$

Therefore, Spearman's correlation coefficient is defined as follows (Equation (5)):

$$R_s = \frac{\sum_{i=1}^{n} (R_i - \bar{R})(S_i - \bar{S})}{\sqrt{\sum_{i=1}^{n} (R_i - \bar{R})^2} \sqrt{\sum_{i=1}^{n} (S_i - \bar{S})^2}} \tag{5}$$

Kendall's correlation coefficient is also computed as follows:

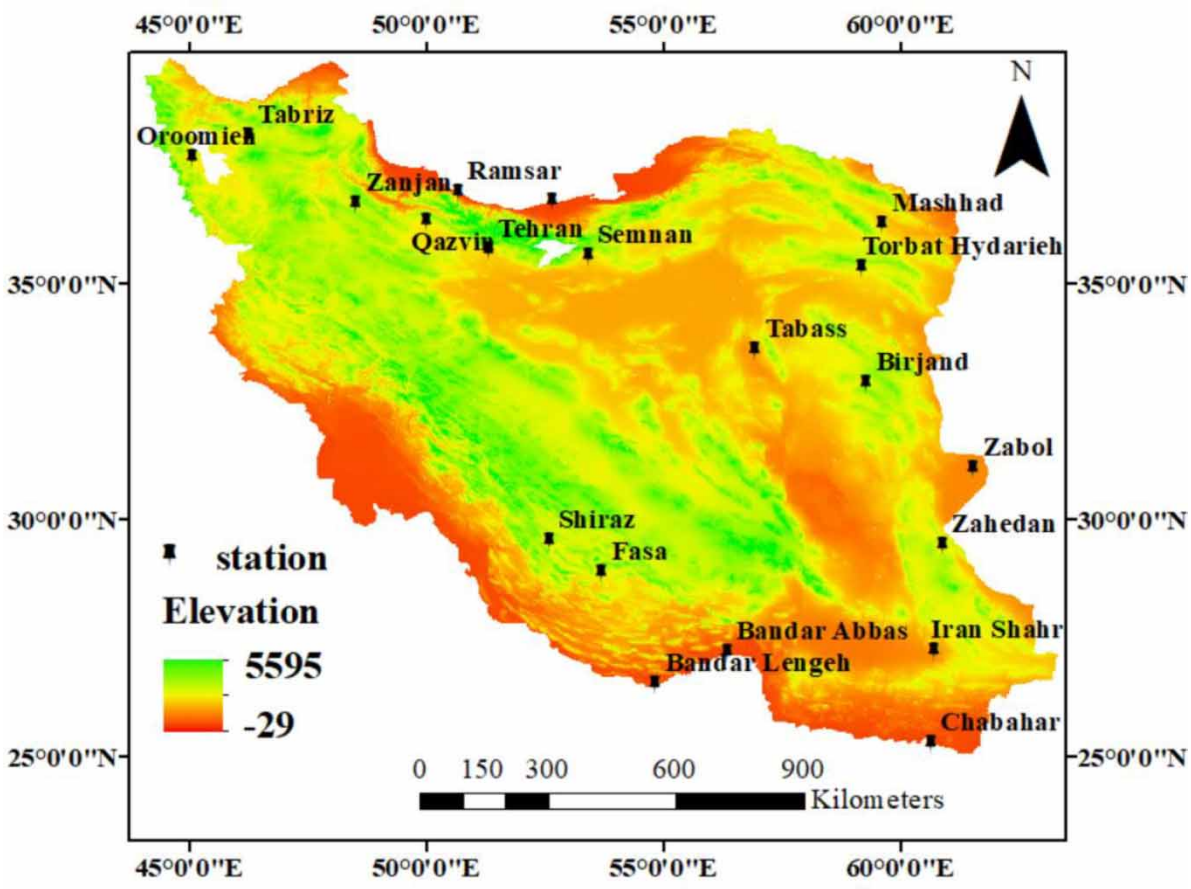

Figure 1 | Study region, selected stations, and their spatial distribution.

The pairs (X_i, Y_i) and (X_j, Y_j) are called concordant, if $X_i - X_j$ and $Y_i - Y_j$ have the same sign (both + or both −). Otherwise, (X_i, Y_i) and (X_j, Y_j) are named discordant. If we show the number of concordant and discordant pairs with A and B, respectively, Kendall's correlation coefficient is calculated as (Equations (6) and (7)):

$$\tau = \frac{A - B}{n(n-1)/2} \tag{6}$$

In other words, we have:

$$\tau = \frac{\sum_{i=1}^{n} \sum_{j=i}^{n} \mathrm{Sgn}((X_i - X_j)(Y_i - Y_j))}{n(n-1)/2} \tag{7}$$

where Sgn(.) is sign function.

The Sen's slope trend is defined as follows:

First, a set of linear slopes is calculated as (Equation (8)):

$$d_{ij} = \frac{y_j - y_i}{x_j - x_i} \tag{8}$$

for $1 \leq i < j \leq n$. Sen's slope is then calculated as the median from all slopes (Equation (9)):

$$\text{Sen's slope} = \text{median}\ (d_{ij}) \tag{9}$$

Table 1 | Geographical location of selected stations and their meteorological characteristics

Station	Latitude (N)	Longitude (E)	Elevation (m a.s.l)	Rainfall (mm/year)	Annual average temperature (°C)	PET (mm/day)
Babolsar	36.720	52.653	− 21.00	917.05	17.35	3.13
Bandar Abbas	27.214	56.373	9.80	173.95	26.98	6.58
Bandar Lengeh	26.528	54.828	22.70	134.13	26.86	6.78
Birjand	32.891	59.283	1491.00	160.68	16.49	5.70
Chabahar	25.281	60.651	8.00	113.20	26.33	5.60
Fasa	28.899	53.719	1268.00	285.55	19.43	5.10
Qazvin	36.319	50.020	1279.10	319.47	14.07	4.19
Iran Shahr	27.229	60.718	591.10	109.82	26.95	6.47
Mashhad	36.236	59.631	999.20	255.32	14.80	4.52
Oroomieh	37.659	45.055	1328.00	330.65	11.36	3.72
Ramsar	36.904	50.683	− 20.00	1232.50	16.29	2.81
Semnan	35.588	53.421	1127.00	139.86	18.29	6.56
Shiraz	29.561	52.603	1488.00	319.11	18.08	5.29
Tabass	33.603	56.951	711.00	82.10	22.16	5.15
Tabriz	38.122	46.242	1361.00	274.55	12.88	4.69
Tehran	35.693	51.309	1191.00	236.82	17.79	5.17
Torbat Hydarieh	35.332	59.206	1451.00	261.22	14.40	5.68
Zabol	31.089	61.543	489.20	54.58	22.41	9.24
Zahedan	29.472	60.900	1370.00	78.44	18.72	6.31
Zanjan	36.660	48.522	1659.40	303.57	11.26	2.68

Note: PET is potential evapotranspiration (calculated based on FAO Penman-Monteith).

2.3. Cross-correlation function

For assessing the relationship of two time series X_t and Y_t, the cross-correlation function (CCF, in abbreviation) is suggested. For two continuous functions f and g, the CCF in lag τ is represented as (Equation (10)):

$$(f*g)(\tau) = \int_{-\infty}^{\infty} f^*(t)g(t+\tau)dt \tag{10}$$

Such that f^* is the complex conjugate of the function f. For two discrete functions f and g, the CCF in lag τ is also represented as (Equation (11)):

$$(f*g)(\tau) = \sum_{t=-\infty}^{\infty} f^*(t)g(t+\tau) \tag{11}$$

As we can observe, the CCF is the rate of the similarity (correlation) of the function f in (t) and the function g in $(t+\tau)$.

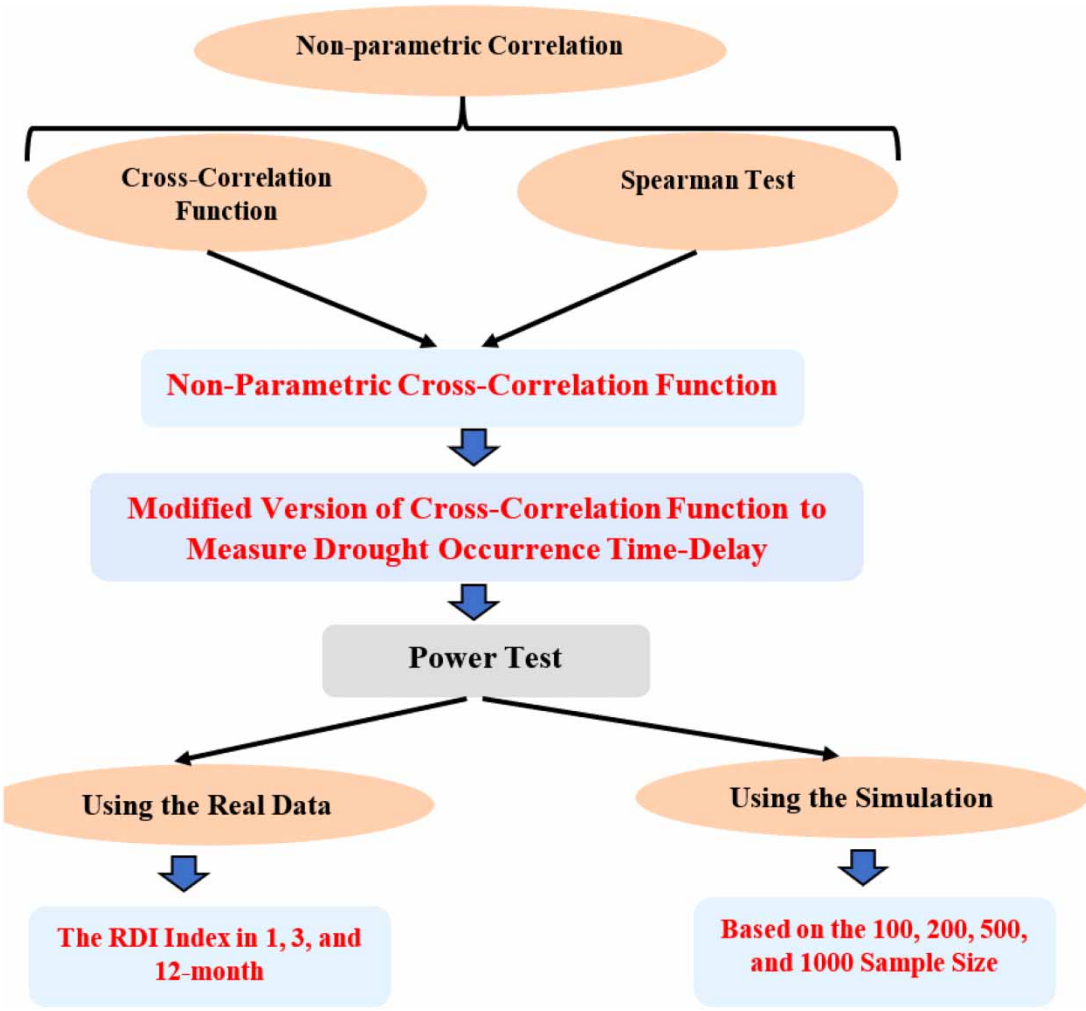

Figure 2 | Flowchart of the research.

If X_t and Y_t are two weak stationary processes, CCF in lag τ is represented as (Equations (12) and (13)):

$$\rho_{X,Y}(\tau) = \mathrm{Corr}(X_t, Y_{t+\tau}) = \frac{\gamma_{X,Y}(\tau)}{\sigma_X \sigma_Y} \tag{12}$$

such that

$$\gamma_{X,Y}(\tau) = E(X_t - \mu_X)(Y_{t+\tau} - \mu_Y) \tag{13}$$

denotes the cross-covariance function (CVF, in abbreviation) of X_t and Y_t in lag τ ($Y_{t+\tau}$), μ_X and μ_Y are the means of X_t and Y_t, and σ_X and σ_Y are respectively the standard deviations of X_t and Y_t.

Usually, the $\rho_{X,Y}(\tau)$ is unknown, and therefore, it should be estimated by using sample realizations of X_t and Y_t. If $\{X_1, \ldots, X_n\}$ and $\{Y_1, \ldots, Y_n\}$ is a path of X_t and Y_t, respectively, the $\rho_{X,Y}(\tau)$ can be estimated by the sample CCF as (Equations (14) and (15):

$$\hat{\rho}_{X,Y}(\tau) = \widehat{\mathrm{Corr}}(X_t, Y_{t+\tau}) = \frac{\hat{\gamma}_{X,Y}(\tau)}{s_X s_Y} \tag{14}$$

Table 2 | The power of $\hat{\pi}_{CCF}$ and $\hat{\pi}_{SCCF}$ for standard Gaussian time series

		n											
		100		**200**		**500**		**1,000**		**MAE**		**RMSE**	
α	τ	$\hat{\pi}_{SCCF}$	$\hat{\pi}_{CCF}$	$\hat{\pi}_{SCCF}$	$\hat{\pi}_{CCF}$	$\hat{\pi}_{SCCF}$	$\hat{\pi}_{CCF}$	$\hat{\pi}_{SCCF}$	$\hat{\pi}_{CCF}$	**SCCF**	**CCF**	**SCCF**	**CCF**
0.1	0	0.989	0.991	0.998	0.994	0.972	0.983	0.986	0.981	0.014	0.013	0.017	0.014
	1	0.983	0.994	0.985	0.982	0.996	0.971	0.987	0.982	0.012	0.018	0.013	0.020
	2	0.963	0.960	0.963	0.987	0.983	0.971	0.984	0.996	0.027	0.022	0.029	0.026
	3	0.986	0.960	0.991	0.962	1.000	0.993	0.982	0.994	0.010	0.023	0.009	0.028
	4	0.952	0.991	0.986	0.979	0.998	0.988	0.986	0.982	0.020	0.015	0.018	0.016
0.3	0	0.957	0.974	0.969	0.991	0.982	0.980	0.993	0.998	0.025	0.014	0.020	0.017
	1	0.979	0.972	0.963	0.986	0.990	0.977	0.988	0.997	0.020	0.017	0.016	0.019
	2	0.982	0.973	0.982	0.999	0.989	0.990	0.992	0.996	0.014	0.011	0.010	0.015
	3	0.986	0.955	0.988	0.985	0.992	0.979	0.982	0.993	0.013	0.022	0.010	0.026
	4	0.993	0.971	0.962	0.996	0.970	0.976	0.997	0.991	0.020	0.017	0.017	0.019
0.5	0	0.950	0.954	0.961	0.992	0.978	0.977	0.985	0.983	0.032	0.024	0.024	0.027
	1	0.968	0.959	0.974	0.968	0.986	0.980	0.987	0.997	0.021	0.024	0.016	0.028
	2	0.998	0.970	0.975	0.999	0.989	0.978	0.993	0.980	0.011	0.018	0.010	0.021
	3	0.961	0.996	0.974	0.972	0.997	0.986	0.999	0.990	0.017	0.014	0.017	0.017
	4	0.997	0.987	0.984	0.983	0.988	0.988	0.994	0.985	0.009	0.014	0.007	0.014
0.7	0	0.994	0.993	0.980	0.999	0.988	0.999	0.998	0.994	0.010	0.004	0.009	0.005
	1	0.961	0.956	0.994	0.972	0.973	0.982	0.986	0.995	0.022	0.024	0.018	0.028
	2	0.977	0.951	0.979	0.977	0.998	0.986	0.991	0.981	0.014	0.026	0.011	0.030
	3	0.992	0.973	0.992	0.986	0.993	0.981	0.991	0.988	0.008	0.018	0.006	0.019
	4	0.990	0.985	0.975	0.972	0.994	0.992	0.988	0.980	0.013	0.018	0.011	0.019
0.9	0	0.971	0.970	0.991	0.977	0.970	0.979	0.995	0.989	0.018	0.021	0.015	0.022
	1	0.959	0.970	0.968	0.962	0.991	0.999	0.995	0.984	0.022	0.021	0.019	0.026
	2	0.958	0.957	0.989	0.979	0.997	0.977	0.985	0.982	0.018	0.026	0.016	0.028
	3	0.977	0.995	0.963	0.977	0.995	0.991	0.984	0.984	0.020	0.013	0.017	0.015
	4	0.954	0.972	0.964	0.999	0.977	0.978	0.993	0.999	0.028	0.013	0.022	0.018
MAE		0.025	0.027	0.022	0.017	0.013	0.017	0.010	0.011				
RMSE		0.042	0.046	0.030	0.020	0.011	0.016	0.006	0.008				

such that

$$\hat{\gamma}_{X,Y}(\tau) = \frac{1}{n}\sum_{t=1}^{n-|\tau|}(X_t - \bar{X})(Y_{t+\tau} - \bar{Y}) \tag{15}$$

is the sample CVF of $\{X_1, \ldots, X_n\}$ and $\{Y_1, \ldots, Y_n\}$ in lag τ, $\bar{X}$ and $\bar{Y}$ are the means of the two realizations, and s_X and s_Y are respectively the standard deviations of the two realizations.

CCF and sample CCF are important tools to measure the rate of time-delay correlation (that is from -1 to $+1$) between two time series.

2.4. Non-parametric cross-correlation function

The CCF, similar to Pearson's correlation, is somewhat sensitive to the normality assumption. In other words, for abnormal populations or populations with outliers, CCF may not work well. To solve this issue, we define a non-parametric CCF (NCCF, in abbreviation), called Spearman's CCF (SCCF, in abbreviation).

If X_t and Y_t are two stationary time series, SCCF in lag τ is defined as following (Equation (16)):

Consider the pairs

$$(X_1, Y_{1+\tau}), \ldots, (X_{n-\tau}, Y_n) \tag{16}$$

Table 3 | The power of $\hat{\pi}_{CCF}$ and $\hat{\pi}_{SCCF}$ for standard uniform time series

		n											
		100		200		500		1,000		MAE		RMSE	
α	τ	$\hat{\pi}_{SCCF}$	$\hat{\pi}_{CCF}$	$\hat{\pi}_{SCCF}$	$\hat{\pi}_{CCF}$	$\hat{\pi}_{SCCF}$	$\hat{\pi}_{CCF}$	$\hat{\pi}_{SCCF}$	$\hat{\pi}_{CCF}$	SCCF	CCF	SCCF	CCF
0.1	0	0.964	0.942	0.984	0.929	0.994	0.928	0.982	0.942	0.019	0.065	0.022	0.065
	1	0.964	0.935	0.988	0.923	0.984	0.936	0.992	0.939	0.018	0.067	0.021	0.067
	2	0.987	0.930	0.974	0.914	0.997	0.938	0.995	0.936	0.012	0.071	0.015	0.071
	3	0.991	0.947	0.977	0.916	0.975	0.929	0.983	0.943	0.019	0.066	0.014	0.067
	4	0.965	0.927	0.980	0.927	0.979	0.943	0.996	0.936	0.020	0.067	0.016	0.067
0.3	0	0.993	0.918	0.967	0.916	0.980	0.920	0.990	0.936	0.018	0.078	0.014	0.078
	1	0.960	0.910	0.978	0.942	0.984	0.930	0.987	0.941	0.023	0.069	0.018	0.070
	2	0.959	0.917	0.967	0.912	0.970	0.945	0.995	0.933	0.027	0.073	0.021	0.074
	3	0.972	0.915	0.974	0.915	0.995	0.923	0.989	0.944	0.018	0.076	0.014	0.077
	4	0.989	0.908	0.961	0.936	0.978	0.945	0.993	0.939	0.020	0.068	0.016	0.069
0.5	0	0.968	0.925	0.964	0.923	0.977	0.930	0.988	0.930	0.026	0.073	0.019	0.073
	1	0.996	0.941	0.992	0.927	0.990	0.924	0.992	0.949	0.008	0.065	0.006	0.066
	2	0.986	0.924	0.963	0.930	0.992	0.930	0.982	0.931	0.019	0.071	0.016	0.071
	3	0.973	0.915	0.998	0.910	0.998	0.924	0.997	0.944	0.009	0.077	0.010	0.078
	4	0.998	0.917	0.982	0.939	0.997	0.950	0.994	0.948	0.007	0.062	0.007	0.063
0.7	0	0.996	0.909	1.000	0.932	0.989	0.930	0.985	0.945	0.008	0.071	0.007	0.072
	1	0.987	0.920	0.977	0.930	0.987	0.934	1.000	0.937	0.012	0.070	0.010	0.070
	2	0.964	0.914	0.995	0.929	0.988	0.940	0.986	0.944	0.017	0.068	0.014	0.069
	3	0.950	0.938	0.961	0.925	0.981	0.947	0.997	0.941	0.028	0.062	0.023	0.063
	4	0.987	0.940	0.986	0.936	0.989	0.935	0.992	0.949	0.012	0.060	0.008	0.060
0.9	0	0.994	0.938	0.969	0.914	0.975	0.934	0.989	0.936	0.018	0.070	0.015	0.070
	1	0.988	0.907	0.961	0.940	0.988	0.935	0.988	0.933	0.019	0.071	0.016	0.072
	2	0.951	0.921	0.979	0.913	0.974	0.944	0.990	0.933	0.027	0.072	0.021	0.073
	3	0.952	0.930	0.967	0.924	0.974	0.927	0.981	0.947	0.032	0.068	0.024	0.069
	4	0.951	0.939	0.991	0.929	0.971	0.948	0.999	0.934	0.022	0.063	0.020	0.063
MAE		0.025	0.027	0.022	0.017	0.013	0.017	0.010	0.011				
RMSE		0.042	0.046	0.030	0.020	0.011	0.016	0.006	0.008				

Sort $X_1, \ldots, X_n$ and $Y_{1+\tau}, \ldots, Y_n$, separately, from smallest to largest. The SCCF in lag τ is defined as the Pearson's correlation coefficient of (Equations (17)–(19)):

$$(R_1, S_1), \ldots, (R_{n-\tau}, S_{n-\tau}) \tag{17}$$

where

$$R_i = rank(X_i) \tag{18}$$

and

$$S_i = rank(Y_{i+\tau}) \tag{19}$$

Therefore, SCCF is defined as following (Equation (20)):

$$\mathrm{SCCF}(\tau) = \frac{\sum_{i=1}^{n-\tau}(R_i - \bar{R})(S_i - \bar{S})}{\sqrt{\sum_{i=1}^{n-\tau}(R_i - \bar{R})^2}\sqrt{\sum_{i=1}^{n-\tau}(S_i - \bar{S})^2}} \tag{20}$$

Table 4 | The power of $\hat{\pi}_{CCF}$ and $\hat{\pi}_{SCCF}$ for exponential (with mean 1) time series

		n											
		100		**200**		**500**		**1,000**		**MAE**		**RMSE**	
α	τ	$\hat{\pi}_{SCCF}$	$\hat{\pi}_{CCF}$	$\hat{\pi}_{SCCF}$	$\hat{\pi}_{CCF}$	$\hat{\pi}_{SCCF}$	$\hat{\pi}_{CCF}$	$\hat{\pi}_{SCCF}$	$\hat{\pi}_{CCF}$	**SCCF**	**CCF**	**SCCF**	**CCF**
0.1	0	0.993	0.921	0.984	0.931	0.987	0.921	0.994	0.934	0.011	0.073	0.011	0.073
	1	0.975	0.949	0.967	0.930	0.989	0.925	0.985	0.943	0.021	0.063	0.023	0.064
	2	0.970	0.937	0.981	0.931	0.987	0.946	0.981	0.948	0.020	0.060	0.021	0.060
	3	0.960	0.935	0.998	0.937	0.990	0.924	0.998	0.945	0.014	0.065	0.015	0.065
	4	0.965	0.930	0.986	0.935	0.990	0.930	0.985	0.949	0.019	0.064	0.015	0.064
0.3	0	0.990	0.920	0.969	0.938	0.982	0.932	0.992	0.937	0.017	0.068	0.013	0.069
	1	0.974	0.945	0.972	0.941	0.976	0.948	0.993	0.947	0.021	0.055	0.016	0.055
	2	0.969	0.935	0.973	0.935	0.987	0.933	0.988	0.949	0.021	0.062	0.016	0.062
	3	0.965	0.948	0.986	0.926	0.987	0.936	0.982	0.947	0.020	0.061	0.015	0.061
	4	0.971	0.900	0.970	0.945	0.995	0.945	0.985	0.946	0.020	0.066	0.016	0.069
0.5	0	0.965	0.949	0.974	0.917	0.987	0.921	0.982	0.950	0.023	0.066	0.017	0.068
	1	0.976	0.928	0.981	0.937	0.972	0.934	0.994	0.931	0.019	0.067	0.015	0.068
	2	0.969	0.901	0.972	0.923	0.997	0.946	0.987	0.949	0.019	0.070	0.016	0.073
	3	0.957	0.933	0.961	0.940	0.991	0.934	0.990	0.942	0.025	0.063	0.021	0.063
	4	0.984	0.947	0.972	0.937	0.981	0.930	0.996	0.940	0.017	0.062	0.013	0.062
0.7	0	0.980	0.911	0.990	0.918	0.996	0.948	0.980	0.946	0.014	0.069	0.011	0.071
	1	0.953	0.906	0.973	0.912	0.978	0.932	0.994	0.934	0.026	0.079	0.021	0.080
	2	0.994	0.914	0.986	0.934	0.979	0.948	0.990	0.931	0.013	0.068	0.010	0.069
	3	0.992	0.908	0.964	0.932	0.983	0.927	0.981	0.948	0.020	0.071	0.016	0.073
	4	0.971	0.919	0.983	0.950	0.994	0.929	0.984	0.949	0.017	0.063	0.013	0.065
0.9	0	0.966	0.939	0.995	0.942	0.992	0.932	0.995	0.950	0.013	0.059	0.013	0.060
	1	0.957	0.934	0.985	0.941	0.999	0.921	0.981	0.936	0.020	0.067	0.017	0.067
	2	0.972	0.919	0.997	0.918	0.981	0.949	0.985	0.946	0.016	0.067	0.013	0.069
	3	0.977	0.925	0.988	0.941	0.978	0.929	0.987	0.947	0.018	0.065	0.013	0.065
	4	0.999	0.933	0.991	0.922	0.980	0.927	0.982	0.934	0.012	0.071	0.010	0.071
MAE		0.025	0.027	0.022	0.017	0.013	0.017	0.010	0.011				
RMSE		0.042	0.046	0.030	0.020	0.011	0.016	0.006	0.008				

2.5. Power test of SCCF

2.5.1. Power test of SCCF based on the simulation

In this section, the ability of the SCCF to detect a time-delay correlation between two stationary time series is studied. For this purpose, numerous datasets from two stationary time series X_t and Y_t with time delay τ are produced and analyzed.

The simulation procedure is as follows:

Step 1: For fixed $n \in \{100,\ 200,\ 500,\ 1,\ 000\}$, a path of size n from X_t is produced. To investigate the impacts of signal class and data length on the applied mathematical techniques functionality over the data, different distributions such as standard normal, standard uniform, Gaussian, non-Gaussian, Brownian motion and fractional Brownian motion, and exponential with different lengths are considered (Fattahi *et al.* 2011; Mitková 2019; Han *et al.* 2022).

Step 2: For fixed time-delay τ, a path of size $n - \tau$ from Y_t is produced by (Equation (21))

$$Y_t = \alpha X_{t-\tau} + Z_t, \quad t = \tau + 1, \ \ldots, n \tag{21}$$

where Z_t is a random sample of size $n - \tau$ from standard normal and $\alpha \in \{0.1,\ 0.3,\ 0.5, 0.7, 0.9\}$.

Step 3: For the time series X_t and Y_t, τ is estimated by CCF and SCCF, as follows (Equations (22) and (23)):

$$\hat{\tau}_{\mathrm{CCF}} = \mathrm{argmax}(\mathrm{CCF}(\tau)) \tag{22}$$

$$\hat{\tau}_{\mathrm{SCCF}} = \mathrm{argmax}(\mathrm{SCCF}(\tau)) \tag{23}$$

Table 5 | The power of $\hat{\pi}_{\mathrm{CCF}}$ and $\hat{\pi}_{\mathrm{SCCF}}$ for Brownian motion time series

		n											
		100		**200**		**500**		**1,000**		**MAE**		**RMSE**	
α	τ	$\hat{\pi}_{\mathrm{SCCF}}$	$\hat{\pi}_{\mathrm{CCF}}$	$\hat{\pi}_{\mathrm{SCCF}}$	$\hat{\pi}_{\mathrm{CCF}}$	$\hat{\pi}_{\mathrm{SCCF}}$	$\hat{\pi}_{\mathrm{CCF}}$	$\hat{\pi}_{\mathrm{SCCF}}$	$\hat{\pi}_{\mathrm{CCF}}$	**SCCF**	**CCF**	**SCCF**	**CCF**
0.1	0	0.965	0.928	0.978	0.932	0.995	0.934	0.991	0.934	0.018	0.068	0.021	0.068
	1	0.972	0.951	0.973	0.950	0.981	0.956	0.981	0.956	0.023	0.047	0.024	0.047
	2	0.970	0.931	0.978	0.938	0.987	0.947	0.992	0.951	0.018	0.058	0.020	0.059
	3	0.976	0.936	0.978	0.938	0.989	0.944	0.989	0.950	0.017	0.058	0.013	0.058
	4	0.978	0.943	0.986	0.908	0.989	0.930	0.992	0.946	0.014	0.068	0.010	0.070
0.3	0	0.965	0.917	0.985	0.930	0.994	0.938	0.997	0.947	0.015	0.067	0.014	0.068
	1	0.965	0.907	0.970	0.943	0.997	0.949	0.998	0.949	0.018	0.063	0.016	0.065
	2	0.968	0.903	0.968	0.929	0.972	0.949	0.986	0.961	0.027	0.065	0.019	0.068
	3	0.967	0.903	0.976	0.904	0.976	0.912	0.980	0.963	0.025	0.080	0.018	0.083
	4	0.963	0.925	0.978	0.937	0.982	0.941	0.998	0.955	0.020	0.061	0.017	0.061
0.5	0	0.950	0.934	0.963	0.942	0.978	0.953	0.984	0.961	0.031	0.053	0.024	0.054
	1	0.967	0.948	0.980	0.957	0.985	0.964	0.991	0.969	0.019	0.041	0.015	0.041
	2	0.963	0.925	0.974	0.943	0.981	0.944	0.986	0.956	0.024	0.058	0.018	0.059
	3	0.962	0.909	0.975	0.918	0.985	0.935	0.992	0.955	0.022	0.071	0.017	0.073
	4	0.990	0.918	0.995	0.956	0.995	0.964	0.998	0.969	0.006	0.048	0.004	0.052
0.7	0	0.978	0.912	0.987	0.939	0.991	0.941	0.994	0.965	0.013	0.061	0.010	0.064
	1	0.974	0.901	0.980	0.926	0.988	0.939	0.995	0.960	0.016	0.069	0.012	0.072
	2	0.957	0.919	0.978	0.933	0.991	0.958	0.997	0.961	0.019	0.057	0.017	0.060
	3	0.931	0.955	0.961	0.963	0.989	0.964	0.998	0.972	0.030	0.037	0.028	0.037
	4	0.968	0.952	0.973	0.955	0.973	0.955	0.992	0.962	0.024	0.044	0.018	0.044
0.9	0	0.966	0.919	0.979	0.925	0.984	0.932	0.995	0.942	0.019	0.071	0.015	0.071
	1	0.973	0.904	0.976	0.940	0.989	0.947	0.992	0.958	0.018	0.063	0.014	0.066
	2	0.968	0.932	0.972	0.934	0.981	0.944	0.995	0.963	0.021	0.057	0.017	0.058
	3	0.952	0.938	0.971	0.943	0.990	0.954	0.997	0.959	0.023	0.052	0.020	0.052
	4	0.965	0.929	0.974	0.933	0.986	0.965	0.995	0.967	0.020	0.052	0.016	0.054
MAE		0.025	0.027	0.022	0.017	0.013	0.017	0.010	0.011				
RMSE		0.042	0.046	0.030	0.020	0.011	0.016	0.006	0.008				

In other words, $\hat{\tau}_{CCF}$ and $\hat{\tau}_{SCCF}$ are the values of τ that have the maximum values of CCF and SCCF, respectively.

Step 4: Steps 1 to 3 are repeated 1,000 times.

Step 5: The power of these approaches ($\hat{\pi}$) are evaluated by (Equations (24) and (25)):

$$\hat{\pi}_{CCF} = \frac{T_{CCF}}{1,000} \tag{24}$$

and

$$\hat{\pi}_{SCCF} = \frac{T_{SCCF}}{1,000} \tag{25}$$

where T_{CCF} and T_{SCCF} are the counts of the cases that $\hat{\tau}_{CCF} = \tau$ and $\hat{\tau}_{SCCF} = \tau$, respectively.

Step 5: Calculating the mean absolute error (MAE) and root mean square error (RMSE) indices for CCF and SCCF methods.

2.6. Power test of SCCF based on the real data

In this section, the ability of SCCF in practice is investigated by an actual example. For this purpose, calculated RDI in 1, 3, and 12-month time scales were used. For investigating the stationarity of the datasets, the augmented Dickey–Fuller (ADF)

Table 6 | The power of $\hat{\pi}_{CCF}$ and $\hat{\pi}_{SCCF}$ for fractional Brownian motion time series

		n											
		100		**200**		**500**		**1,000**		**MAE**		**RMSE**	
α	τ	$\hat{\pi}_{SCCF}$	$\hat{\pi}_{CCF}$	$\hat{\pi}_{SCCF}$	$\hat{\pi}_{CCF}$	$\hat{\pi}_{SCCF}$	$\hat{\pi}_{CCF}$	$\hat{\pi}_{SCCF}$	$\hat{\pi}_{CCF}$	**SCCF**	**CCF**	**SCCF**	**CCF**
0.1	0	0.965	0.929	0.974	0.933	0.986	0.965	0.995	0.967	0.020	0.052	0.023	0.054
	1	0.974	0.915	0.986	0.924	0.990	0.941	0.993	0.956	0.014	0.066	0.016	0.068
	2	0.966	0.939	0.968	0.943	0.995	0.946	0.997	0.955	0.019	0.054	0.024	0.055
	3	0.969	0.939	0.973	0.945	0.978	0.954	0.997	0.962	0.021	0.050	0.017	0.051
	4	0.972	0.927	0.980	0.933	0.985	0.949	0.994	0.959	0.017	0.058	0.013	0.059
0.3	0	0.968	0.935	0.975	0.937	0.982	0.951	0.989	0.959	0.022	0.055	0.016	0.055
	1	0.973	0.936	0.981	0.947	0.991	0.956	0.992	0.961	0.016	0.050	0.012	0.051
	2	0.966	0.937	0.980	0.942	0.989	0.953	0.999	0.965	0.017	0.051	0.014	0.052
	3	0.968	0.936	0.979	0.943	0.983	0.958	0.993	0.969	0.019	0.049	0.015	0.050
	4	0.960	0.935	0.982	0.936	0.987	0.961	0.992	0.969	0.020	0.050	0.016	0.052
0.5	0	0.976	0.925	0.985	0.938	0.991	0.956	0.993	0.966	0.014	0.054	0.011	0.056
	1	0.970	0.929	0.983	0.934	0.990	0.941	0.990	0.956	0.017	0.060	0.013	0.061
	2	0.958	0.915	0.971	0.935	0.989	0.943	0.997	0.959	0.021	0.062	0.018	0.064
	3	0.963	0.919	0.973	0.934	0.987	0.941	0.995	0.964	0.021	0.061	0.017	0.063
	4	0.965	0.925	0.969	0.931	0.987	0.945	0.995	0.958	0.021	0.060	0.017	0.062
0.7	0	0.970	0.933	0.982	0.942	0.993	0.952	0.998	0.964	0.014	0.052	0.013	0.054
	1	0.966	0.915	0.987	0.926	0.992	0.939	0.994	0.942	0.015	0.070	0.013	0.070
	2	0.965	0.929	0.968	0.940	0.985	0.948	0.998	0.955	0.021	0.057	0.018	0.058
	3	0.976	0.930	0.977	0.945	0.989	0.957	0.994	0.961	0.016	0.052	0.013	0.053
	4	0.982	0.922	0.986	0.936	0.989	0.951	0.998	0.963	0.011	0.057	0.009	0.059
0.9	0	0.976	0.923	0.984	0.936	0.989	0.957	0.999	0.960	0.013	0.056	0.011	0.058
	1	0.964	0.932	0.981	0.936	0.982	0.955	0.992	0.961	0.020	0.054	0.016	0.055
	2	0.977	0.930	0.984	0.938	0.987	0.959	1.000	0.966	0.013	0.052	0.011	0.054
	3	0.969	0.928	0.982	0.939	0.992	0.953	0.995	0.965	0.016	0.054	0.013	0.056
	4	0.972	0.926	0.990	0.945	0.991	0.963	0.993	0.968	0.014	0.050	0.011	0.052
MAE		0.025	0.027	0.022	0.017	0.013	0.017	0.010	0.011				
RMSE		0.042	0.046	0.030	0.020	0.011	0.016	0.006	0.008				

and Kwiatkowski–Phillips–Schmidt–Shin (KPSS) tests were applied. These tests verify that the computed RDI in all three time scales were stationary.

2.6.1. Study region, data collection, and data evaluation

In this research, the climatic data series of 20 stations (including Babolsar, Bandar Abbas, Bandar Lengeh, Birjand, Chabahar, Fasa, Qazvin, Iran Shahr, Mashhad, Oroomieh, Ramsar, Semnan, Shiraz, Tabass, Tabriz, Tehran, Torbat Hydarieh, Zabol,

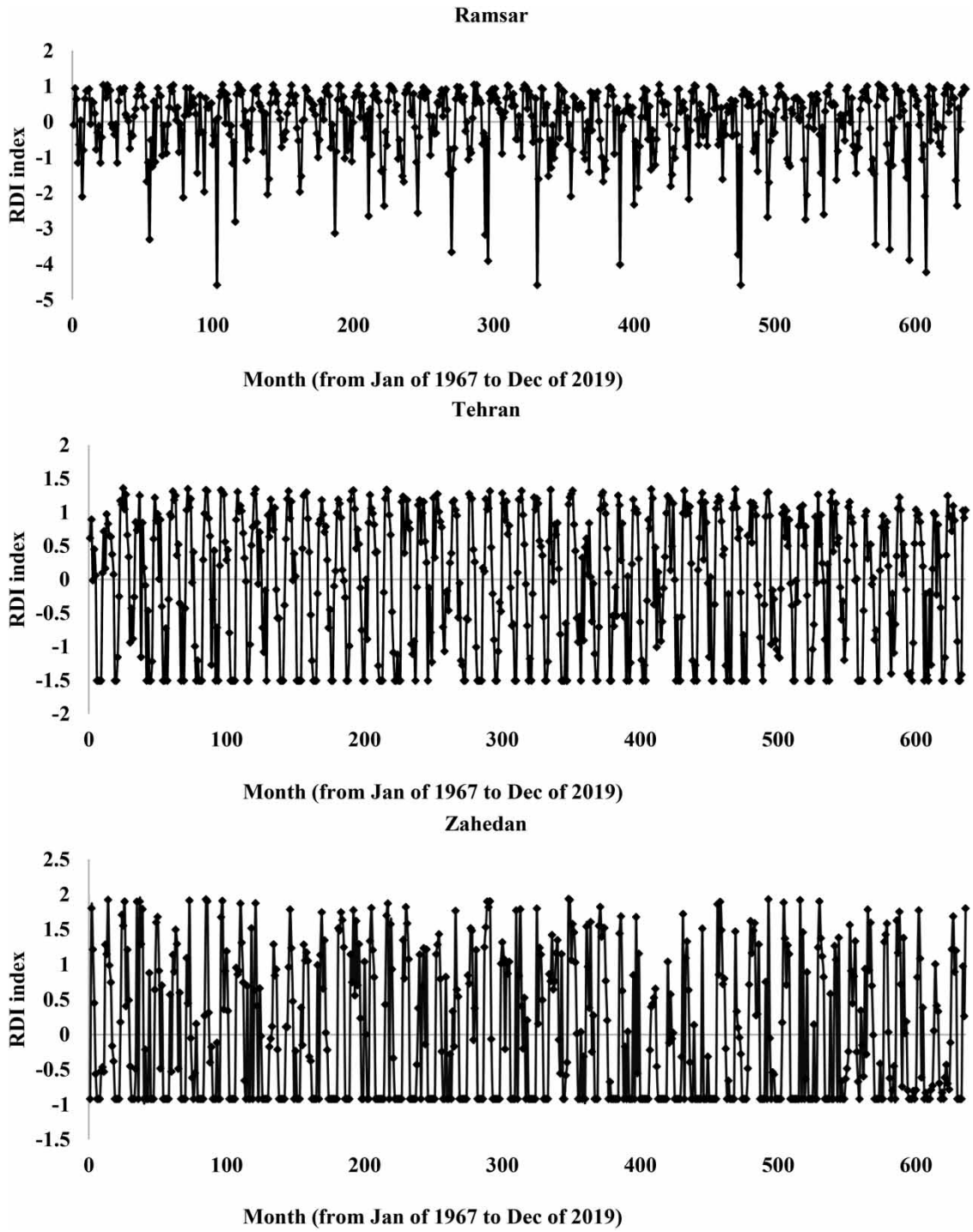

Figure 3 | Calculated monthly (1-month) RDI in some of the selected stations.

Zahedan, and Zanjan stations) with proper spatial distribution, adequacy of the length of the data series, appropriate climate diversity from 1967 to 2019 over Iran were used (Figure 1). Before using data series in all stations, the missing values of the data series were estimated using the Fuzzy regression method (Sadatinejad *et al.* 2011). The length adequacy of the data series (time duration) was evaluated using the Mockus equation (Zarei & Mahmoudi 2021). The Run-test method was used for assessing the homogeneity of the data series (Mahdavi 2002). Then at all stations, the RDI index in different time scales, including monthly (1-month), seasonal (3-month), and annual (12-month), were calculated. According to the purpose and hypothesis of the research (mentioned in the previous sections), in selecting the stations, it was tried to select and use stations

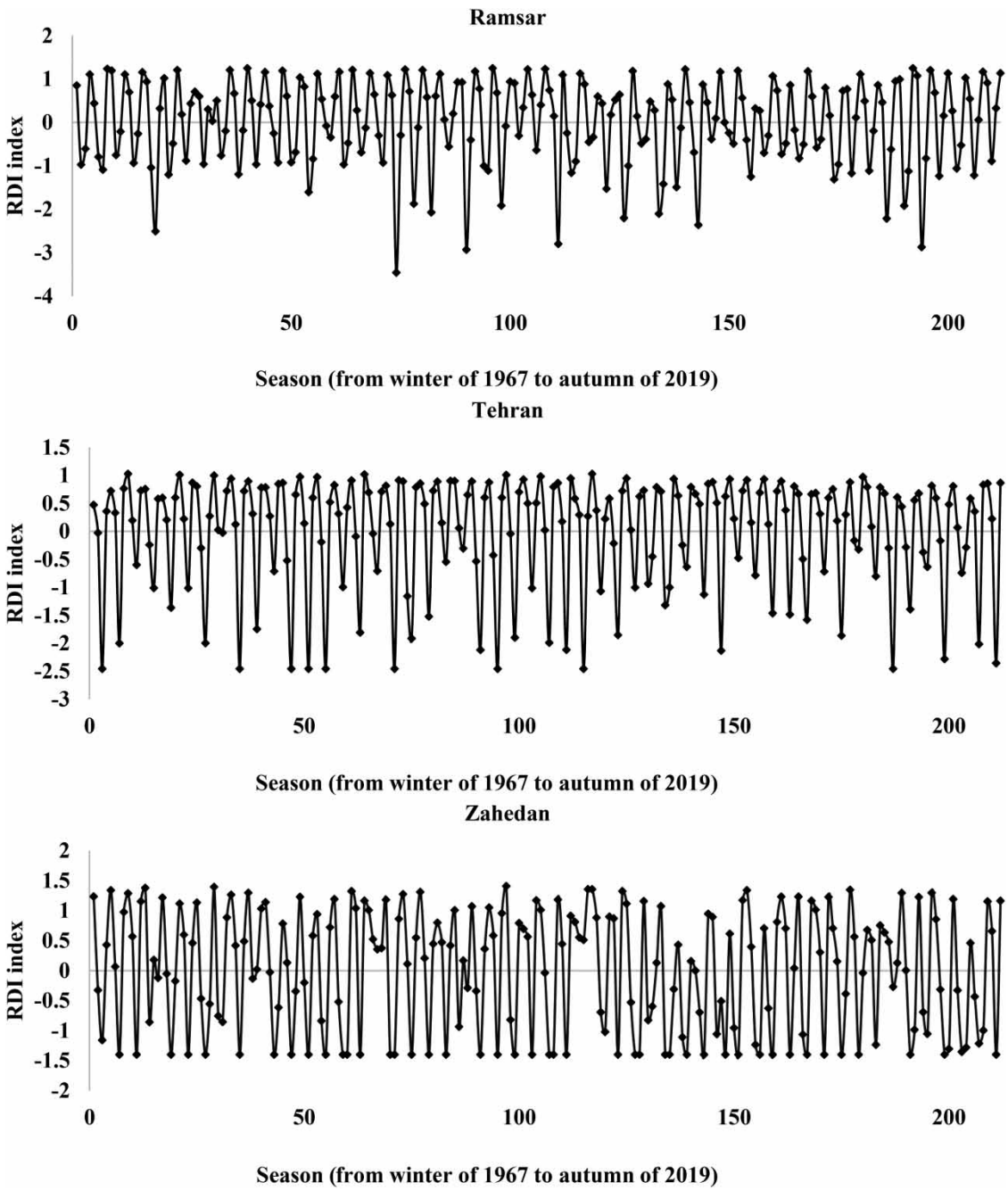

Figure 4 | Calculated seasonal (3-month) RDI in some of the selected stations.

with abnormal RDI data series in 1, 3, and 12-month time scales. Some geographical and meteorological characteristics of chosen stations are presented in Table 1. It should be noted that the required meteorological data were obtained from the Iran Meteorological Organization (www.irimo.ir), and the R 3.6 and SPSS 20 software were used to perform the analysis.

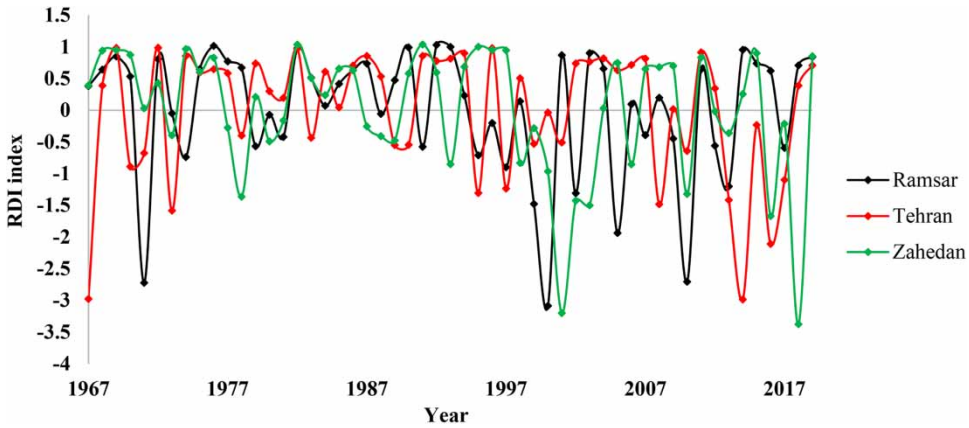

Figure 5 | Calculated annually (12-month) RDI in some of the selected stations.

Table 7 | Results of the normality test of calculated RDI in 1, 3, and 12-month time scales (based on Kolmogorov–Smirnov test)

	12-month (Annual)	3-month (Seasonal)	1-month (monthly)
Station		**Significant level**	
Babolsar	0.0000	0.0000	0.0000
Bandar Abbas	0.0000	0.0000	0.0000
Bandar Lengeh	0.0031	0.0000	0.0000
Birjand	0.0000	0.0000	0.0000
Chabahar	0.0000	0.0000	0.0000
Fasa	0.0000	0.0000	0.0000
Qazvin	0.0030	0.0000	0.0000
Iran Shahr	0.0000	0.0000	0.0000
Mashhad	0.0173	0.0000	0.0000
Oroomieh	0.0105	0.0000	0.0000
Ramsar	0.0024	0.0000	0.0000
Semnan	0.0000	0.0000	0.0000
Shiraz	0.0000	0.0000	0.0000
Tabass	0.0002	0.0000	0.0000
Tabriz	0.0014	0.0000	0.0000
Tehran	0.0001	0.0000	0.0000
Torbat Hydarieh	0.0000	0.0000	0.0000
Zabol	0.0001	0.0000	0.0000
Zahedan	0.0036	0.0000	0.0000
Zanjan	0.0000	0.0000	0.0000

Note: Calculated RDI data series at all station and all time scales were non-normal.

2.6.2. The RDI calculation

The RDI index was introduced by Tsakiris (2004) and is based on the rainfall and potential evapotranspiration (PET) variables. This index was calculated using the following equations (Tsakiris *et al.* 2007; Equations (26) and (27):

$$\mathrm{RDI}_{st}^{i} = \frac{y_k^i - \bar{y}_k}{\hat{\sigma}_{yk}} \tag{26}$$

$$\alpha_k^i = \frac{\sum_{j=1}^{k} P_{ij}}{\sum_{j=1}^{k} \mathrm{PET}_{ij}},\ i = 1{:}N; j = 12 \tag{27}$$

where $\bar{y}_k$ and $\hat{\sigma}_{yk}$ are the arithmetic mean and the standard deviation of y_k respectively, y_k is equal to ln (α_k^i), P_{ij}, and PET_{ij} are respectively the amount of rainfall and PET in month jth of the ith year during the whole N year of study (hydrological year starts from October in Iran). It is suggested to see Lashkari *et al.* (2021), Mohammed & Yimam (2021), and El-Tantawi *et al.* (2021) for more details about the RDI. Some advantages of RDI including: the RDI is a multiscalar index that calculates the

Table 8 | Spearman cross-correlations (SCCF) between calculated annually (12-month) RDI values in groups with stations with low spatial distance

	SCCF									
Lags	**Group 1**	**Group 2**	**Group 3**	**Group 4**	**Group 5**	**Group 6**	**Group 7**	**Group 8**	**Group 9**	**Group 10**
−10	0.0005	0.1049	− 0.0202	0.2995	− 0.0403	0.1082	0.1234	− 0.1101	0.1185	− 0.1329
−9	− 0.0307	0.0443	− 0.0065	0.2463	0.1416	− 0.1320	− 0.0497	− 0.2020	− 0.0040	− 0.0858
−8	− 0.1168	0.2533	− 0.0339	0.3018	− 0.1088	− 0.0138	0.0601	− 0.0543	0.0160	− 0.0364
−7	0.0803	0.1000	0.0288	0.1830	− 0.0510	0.0815	0.1339	0.1147	− 0.0714	− 0.0528
−6	0.0245	0.1347	0.0004	0.1420	0.0950	0.0186	0.2456	− 0.0553	0.0411	− 0.0900
−5	0.0035	0.0029	0.0869	0.2460	− 0.0505	0.1119	0.2367	0.0023	− 0.1538	0.1058
−4	0.0702	0.0819	0.0649	0.1850	0.1297	− 0.0557	0.0347	0.1344	− 0.2147	0.0852
−3	0.0121	− 0.1011	0.1224	0.1245	− 0.0456	0.1338	0.1384	0.0419	− 0.0503	0.1009
−2	0.0951	0.0476	0.2386	0.1611	− 0.1913	0.0019	0.0581	0.3827	− 0.2104	0.1566
−1	− 0.1325	0.1336	0.0397	0.3220	0.0918	0.2396	0.1591	0.1876	− 0.0391	− 0.1055
0	**0.4297**	**0.5673**	**0.8729**	**0.7821**	**0.3120**	**0.6616**	**0.6968**	**0.3965**	**0.5961**	**0.6890**
1	− 0.1149	0.1047	0.0931	0.2272	0.1486	0.0794	0.1338	− 0.0817	− 0.0275	− 0.1269
2	− 0.0568	0.1947	0.1702	0.2074	0.0631	0.1151	0.1174	0.0856	0.0948	0.1294
3	− 0.0810	− 0.0547	0.1493	− 0.0521	− 0.0767	0.1301	− 0.1865	− 0.0649	0.0127	0.2378
4	− 0.0623	− 0.0093	0.0224	0.0975	0.1113	0.1562	0.1326	− 0.1634	− 0.0374	0.0781
5	− 0.3050	− 0.0793	0.0945	0.2404	0.2806	0.1541	0.1126	− 0.1559	− 0.0812	0.3509
6	− 0.0113	0.0185	0.0130	− 0.0191	0.0144	0.0058	0.1522	− 0.1215	− 0.1526	0.0177
7	− 0.1435	− 0.1232	− 0.0400	0.1418	− 0.1067	0.1551	0.2771	− 0.2987	− 0.0980	0.1085
8	0.0107	− 0.1440	0.0628	0.0439	0.1732	− 0.1410	− 0.1135	− 0.1076	− 0.1564	0.1201
9	− 0.1781	− 0.1499	− 0.0630	0.1401	0.0102	0.2065	− 0.0261	− 0.0937	0.0450	− 0.1033
10	0.1346	0.0691	− 0.0632	0.2079	0.2402	0.0120	0.0588	− 0.1474	0.0529	0.0882

Note: Each group includes two adjacent stations (with low spatial distance). Group1 including Fasa and Shiraz stations, group 2 including Zabol and Zahedan stations, group 3 including Bandar Abass and Bandar Lenge stations, group 4 including Oroomieh and Tabriz stations, group 5 including Ramsar and Babolsar stations, group 6 including Birjand and Tabass stations, group 7 including Torbat Hydarieh and Mashhad stations, group 8 including Iran Shahr and Chabahar stations, group 9 including Qazvin and Zanjan stations, and group 10 including Semnan and Tehran stations.
Bold characters are the maximum values of SCCF.

drought severity in different time scales. This index is based on P and PET variables and is sensitive to changes in environmental conditions. A flowchart of the research is presented in Figure 2.

3. RESULTS AND DISCUSSION

3.1. Power test of SCCF based on the simulation

The computed values of $\hat{\pi}$, for different settings of parameter, are presented in Tables 2–4. The results show that the values of $\hat{\pi}_{CCF}$ and $\hat{\pi}_{SCCF}$ are close to each other for Gaussian (normal) time series. Based on Table 2, in $n = 100$, 200, 500, and 1,000 at 64, 60, 64, and 60% of lags the $\hat{\pi}_{SCCF}$ was more than the $\hat{\pi}_{CCF}$, respectively. Presented results in Tables 3 and 4 indicated that at 100% of numerical studies for uniform and exponential time series, the $\hat{\pi}_{SCCF}$ is larger than $\hat{\pi}_{CCF}$. In other words, the SCCF is more robust than the CCF, in detecting time delay between two non-Gaussian time series. Tables 5 and 6 indicate that almost at 100% of numerical studies for Brownian motion time series and fractional Brownian motion time series, the $\hat{\pi}_{SCCF}$ is larger than $\hat{\pi}_{CCF}$. In other words, the SCCF is more robust than the CCF, in detecting time delay. The results of the MAE and RMSE also showed that the SCCF is more robust than the CCF, in detecting time delay.

3.2. Ability assessment of SCCF using the real data

In this section, the ability of SCCF in practice is investigated by an actual example. For this purpose, the calculated data of RDI in 1, 3, and 12-month time scales were used. The ADF and KPSS tests were used to investigate the stationarity of the datasets. The results of the ADF and KPSS tests verify that the calculated RDI in all time scales were stationary.

Table 9 | Spearman cross-correlations (SCCF) between calculated seasonal (3-month) RDI values in groups with stations with low spatial distance

	SCCF									
Lags	**Group 1**	**Group 2**	**Group 3**	**Group 4**	**Group 5**	**Group 6**	**Group 7**	**Group 8**	**Group 9**	**Group 10**
−10	− 0.7360	− 0.5862	− 0.5520	− 0.5898	− 0.7800	− 0.7278	− 0.7676	− 0.1937	− 0.7275	− 0.7269
−9	0.0428	− 0.0306	0.0245	− 0.0367	0.0203	0.1093	0.0059	0.0540	0.0208	0.0140
−8	0.7475	0.6389	0.6299	0.7129	0.7749	0.7444	0.7919	0.3915	0.7744	0.7251
−7	0.0064	0.1026	0.0165	− 0.0076	− 0.0143	− 0.0658	0.0204	− 0.1182	− 0.0625	− 0.0186
−6	− 0.7424	− 0.6635	− 0.5639	− 0.5768	− 0.7684	− 0.7906	− 0.8059	− 0.1550	− 0.7396	− 0.7229
−5	0.0285	− 0.0414	0.0254	− 0.0286	0.0017	0.1055	− 0.0289	0.0354	0.0064	− 0.0017
−4	0.7411	0.5975	0.5693	0.7520	0.8005	0.7605	0.8108	0.4160	0.7891	0.7336
−3	− 0.0202	0.0714	− 0.0103	0.0170	− 0.0143	− 0.0637	0.0263	− 0.0786	− 0.0672	− 0.0190
−2	− 0.7467	− 0.6046	− 0.5533	− 0.6234	− 0.8023	− 0.7444	− 0.8016	− 0.2052	− 0.7405	− 0.7378
−1	0.0221	− 0.0688	0.0162	− 0.0216	0.0090	0.1165	− 0.0066	0.0448	0.0006	0.0341
0	**0.9505**	**0.8668**	**0.8959**	**0.9163**	**0.9015**	**0.9076**	**0.9490**	**0.5419**	**0.9252**	**0.8977**
1	− 0.0236	0.0889	− 0.0238	− 0.0179	− 0.0304	− 0.0817	0.0262	− 0.1146	− 0.0557	− 0.0177
2	− 0.7374	− 0.5869	− 0.5790	− 0.6108	− 0.7950	− 0.7444	− 0.7889	− 0.2621	− 0.7396	− 0.7409
3	0.0480	− 0.0567	0.0439	− 0.0411	0.0408	0.0882	− 0.0097	− 0.0610	0.0025	0.0382
4	0.7322	0.6167	0.5979	0.7450	0.8178	0.7583	0.8053	0.4519	0.7819	0.7545
5	− 0.0014	0.0824	− 0.0004	− 0.0233	− 0.0298	− 0.0695	0.0090	− 0.1389	− 0.0708	− 0.0322
6	− 0.7539	− 0.6606	− 0.6218	− 0.5967	− 0.7882	− 0.7896	− 0.8002	− 0.2217	− 0.7376	− 0.7245
7	0.0217	− 0.0571	− 0.0059	− 0.0395	0.0311	0.1028	− 0.0026	0.0019	0.0165	0.0491
8	0.7188	0.6764	0.6377	0.7331	0.7883	0.7473	0.7849	0.3762	0.7847	0.7572
9	− 0.0218	0.0764	− 0.0244	− 0.0027	− 0.0280	− 0.0881	0.0427	− 0.1812	− 0.0440	− 0.0159
10	− 0.7299	− 0.5909	− 0.5938	− 0.6077	− 0.7710	− 0.7414	− 0.7600	− 0.2742	− 0.7053	− 0.7073

Note: Bold characters are the maximum values of SCCF.

3.2.1. Data collection and evaluation

In this research, the humidity data in 1971 at Tabass were estimated using the Fuzzy regression. Based on the results, the time duration of the data series (Based on the Mockus equation) was significantly adequate at all stations (at a 0.99 significant level). The results of the Run-test indicated that all data series at all stations were homogeneous.

3.2.2. Calculated RDI

Calculated RDI in selected stations at different time scales showed that at all stations and all time scales, the normal class of drought severity (with RDI value between 0.99 and −0.99) had the most occurrence frequency (Figures 3–5). Based on the results, the most severe drought occurred in Babolsar, Bandar Abbas, Bandar Lengeh, Birjand, Chabahar, Fasa, Qazvin, Iran Shahr, Mashhad, Oroomieh, Ramsar, Semnan, Shiraz, Tabass, Tabriz, Tehran, Torbat Hydarieh, Zabol, Zahedan, and Zanjan stations in 2010, 2010, 2001, 2018, 2010, 2010, 2017, 2008, 2000, 2010, 2016, 2016, 2008, 2008, 2001, 1999, 1973, 2014, 2017, and 1967 years, respectively. The main reason for the occurrence of severe droughts in the years mentioned above is a significant decrease in the amount of rainfall. This issue has been confirmed in Zarei *et al.* (2022) research.

3.2.3. Normality test of RDI data series

In this study, the Kolmogorov–Smirnov test was used to assess the normality of the calculated RDI in 1, 3, and 12-month time scales. Based on the results of the normality test, the calculated RDI at all stations and all chosen time scales were non-normal at the 0.05 significant level (Table 7). Table 7 shows that in all stations and all time scales, the calculated significance levels for the Kolmogorov–Smirnov were less than 0.05.

Table 10 | Spearman cross-correlations (SCCF) between calculated monthly (1-month) RDI values in groups with stations with low spatial distance

	SCCF									
Lags	**Group 1**	**Group 2**	**Group 3**	**Group 4**	**Group 5**	**Group 6**	**Group 7**	**Group 8**	**Group 9**	**Group 10**
−10	0.2455	0.2711	0.1482	0.2984	0.3444	0.2795	0.3243	− 0.0039	0.2846	0.2648
−9	− 0.0538	0.0363	− 0.0351	− 0.0438	0.0422	− 0.0281	− 0.0025	− 0.1307	− 0.0720	− 0.0203
−8	− 0.3405	− 0.1914	− 0.2239	− 0.2744	− 0.2814	− 0.3596	− 0.3362	− 0.1850	− 0.3819	− 0.3327
−7	− 0.5113	− 0.3451	− 0.3167	− 0.4641	− 0.5212	− 0.5729	− 0.6202	− 0.1233	− 0.5841	− 0.5384
−6	− 0.5922	− 0.4408	− 0.3648	− 0.5205	− 0.6452	− 0.6372	− 0.7029	− 0.1153	− 0.6520	− 0.6144
−5	− 0.5233	− 0.4117	− 0.3365	− 0.4947	− 0.5760	− 0.5525	− 0.6105	− 0.1083	− 0.5694	− 0.5324
−4	− 0.2904	− 0.2892	− 0.2101	− 0.3397	− 0.3360	− 0.3055	− 0.3594	− 0.1211	− 0.3441	− 0.3173
−3	− 0.0044	− 0.0807	− 0.0494	− 0.0610	− 0.0358	0.0326	0.0041	− 0.0028	− 0.0120	0.0077
−2	0.2970	0.2140	0.2024	0.2996	0.2577	0.3687	0.3519	0.1595	0.3395	0.3459
−1	0.5965	0.4368	0.4275	0.5758	0.5294	0.6599	0.6640	0.3338	0.6497	0.6084
0	**0.9405**	**0.7992**	**0.8767**	**0.8846**	**0.8016**	**0.8669**	**0.9152**	**0.4048**	**0.8983**	**0.8636**
1	0.5642	0.4710	0.4132	0.5697	0.5667	0.5789	0.6487	0.2020	0.6126	0.5763
2	0.2604	0.2969	0.1866	0.2979	0.3577	0.2971	0.3625	− 0.0122	0.3081	0.2959
3	− 0.0476	0.0390	− 0.0687	− 0.0288	0.0158	− 0.0533	0.0060	− 0.1788	− 0.0451	− 0.0056
4	− 0.3178	− 0.1742	− 0.2180	− 0.3092	− 0.2859	− 0.3335	− 0.3357	− 0.2182	− 0.3936	− 0.3454
5	− 0.5251	− 0.3427	− 0.3261	− 0.4508	− 0.5190	− 0.5679	− 0.5997	− 0.1423	− 0.5915	− 0.5636
6	− 0.5927	− 0.4490	− 0.3737	− 0.5216	− 0.6382	− 0.6390	− 0.6887	− 0.1275	− 0.6539	− 0.6272
7	− 0.5166	− 0.3871	− 0.3354	− 0.5066	− 0.5470	− 0.5658	− 0.6158	− 0.1267	− 0.5627	− 0.5230
8	− 0.3194	− 0.2830	− 0.2047	− 0.3260	− 0.3336	− 0.3129	− 0.3477	− 0.1226	− 0.3368	− 0.3145
9	0.0017	− 0.0434	0.0181	− 0.0749	− 0.0359	0.0180	− 0.0140	− 0.0715	− 0.0184	− 0.0206
10	0.3037	0.1686	0.2092	0.2455	0.2809	0.3405	0.3371	0.1136	0.3367	0.3182

Note: Bold characters are the maximum values of SCCF.

3.2.4. SCCF ability assessment

To assess the ability of SCCF using the actual RDI data in 1, 3, and 12-month time scales at first, 15 groups of meteorological stations were defined; 10 out of 15 groups included two stations with short spatial distance, and 5 out of 15 groups included two stations with long spatial distance. Groups with short spatial distance, including group 1 including Fasa and Shiraz stations, group 2 including Zabol and Zahedan stations, group 3 including Bandar Abass and Bandar Lenge stations, group 4 including Oroomieh and Tabriz stations, group 5 including Ramsar and Babolsar stations, group 6 including Birjand and Tabass stations, group 7 including Torbat Hydarieh and Mashhad stations, group 8 including Iran Shahr and Chabahar stations, group 9 including Qazvin and Zanjan stations, and group 10 including Semnan, and Tehran stations and groups with long spatial distance including group 11 including Fasa and Tabriz stations, group 12 including Qazvin and Zahedan stations, group 13 including Bandar Abass and Mashhad stations, group 14 including Oroomieh, and Shiraz stations, and group 15 including Chabahar and Semnan stations. Then the SCCF between the RDI values of two stations in each group at different time scales in 21 lags, including 10, 9, 8, 7, 6, 5, 4, 3, 2, 1, 0, −1, −2, −3, −4, −5, −6, −7, −8, −9, and −10 were estimated. It is expected that, if the SCCF had good ability, the result of SCCF between stations with short spatial distance does not reveal delay time in drought occurrence. In stations with long spatial distances, this result should be reversed.

The results of the SCCF of the calculated RDI data series in groups 1–10, including stations with short spatial distance, indicated that in 1, 3, and 12-month time scales at all groups, the maximum values of SCCF were estimated in lag 0 (Tables 8–10). In other words, in all stations close to each other, the drought occurrence is simultaneous and has no time delay. According to the

Table 11 | Spearman cross-correlations (SCCF) between calculated annually (12-month) RDI values in groups with stations with high spatial distance

	SCCF				
Lags	**Group 11**	**Group 12**	**Group 13**	**Group 14**	**Group 15**
−10	− 0.0668	0.0276	**0.3513**	− 0.0221	0.1147
−9	− 0.2115	− 0.2205	0.0486	− 0.1589	− 0.0097
−8	− 0.2520	0.0413	0.1312	− 0.0187	− 0.1709
−7	− 0.2186	0.0551	0.1971	0.0335	− 0.1040
−6	− 0.3258	0.0734	0.0479	− 0.0526	− 0.1118
−5	− 0.2457	− 0.0065	0.3010	− 0.0851	− 0.1078
−4	− 0.1856	− **0.2342**	0.1299	− **0.3455**	− 0.1568
−3	− 0.3329	0.0059	0.1595	− 0.1185	− 0.0834
−2	− 0.3511	0.0937	0.1868	0.1633	0.0147
−1	− 0.3277	0.1091	0.0972	0.0164	0.0174
0	− 0.1373	0.1957	0.3486	0.2586	0.1058
1	− 0.3702	− 0.1639	0.0564	0.1563	0.1180
2	− 0.2430	0.1877	0.1703	0.1126	0.1327
3	− 0.3586	0.1930	0.0422	0.0409	0.0270
4	− **0.4308**	− 0.0142	0.1813	− 0.2206	**0.2030**
5	− 0.2828	− 0.0188	0.0194	− 0.0577	0.0093
6	− 0.2104	0.0440	0.0994	− 0.0033	0.0233
7	− 0.2756	− 0.1147	0.0860	− 0.0030	0.1517
8	− 0.1661	0.0094	− 0.1831	0.0772	− 0.0103
9	− 0.2960	− 0.0145	0.0470	0.1980	− 0.0270
10	− 0.1275	− 0.0410	0.3056	0.3418	− 0.0342

Note: Each group is including two stations with high spatial distance. Group 11 including Fasa and Tabriz stations, group 12 including Qazvin and Zahedan stations, group 13 including Bandar Abass and Mashhad stations, group 14 including Oroomieh and Shiraz stations, and group 15 including Chabahar and Semnan stations.
Bold characters are the maximum values of SCCF (based on the absolute value).

results of the SCCF of the RDI data series in groups 11–15, including stations with long spatial distances, in 1, 3, and 12-month time scales, at all groups, the occurrence of drought at one station versus another station has time delay (Tables 11–13). This result proves the good ability of the SCCF model. Based on the results, in the monthly time scale, the maximum absolute value of SCCF in groups 11, 12, 13, 14, and 15 occurred in lags 6, 6, −6, 1, and 1, respectively. In the seasonal time scale, the maximum absolute value of SCCF in groups 11, 12, 13, 14, and 15 occurred in lags −4, 2, 4, 4, and 4, respectively. In annual time scale, the maximum absolute value of SCCF in groups 11, 12, 13, 14, and 15 occurred in lags 4, −4, −10, −4, and 4, respectively (Figure 6). It seems the main reason for the greater ability of the SCCF model compared to the CCF model is that the SCCF model is a hybrid model (a hybrid of the Spearman and SSF models). Roustaei *et al.* (2021) assessed the time delay between wind erosion and drought in the Southern regions of Iran using the CCF function. They showed that the maximum CC between drought and wind erosion was equal to −0.22 (without time lag). While the calculated correlation values by the SCCF model in this research were much higher.

4. CONCLUSION

The analysis of environmental, meteorological, and hydrological datasets often requires the detection of relationships between their variables. Generally, for assessing the relationship between two time series datasets, the CCF is suggested. The CCF is somewhat sensitive to the abnormality of datasets and the existence of outliers. Therefore, for abnormal datasets or for datasets with outliers, the CCF may not work well. To solve this issue, in this research, a non-parametric cross-correlation function was defined (SCCF). The ability of the proposed measure to detect the time-delay correlation between two stationary time series was studied. For this purpose, numerous datasets from two stationary time series were produced and

Table 12 | Spearman cross-correlations (SCCF) between calculated seasonal (3-month) RDI values in groups with stations with high spatial distance

	SCCF				
Lags	**Group 11**	**Group 12**	**Group 13**	**Group 14**	**Group 15**
−10	− 0.6587	− 0.6653	− 0.6882	− 0.7068	− 0.5130
−9	0.0231	− 0.1244	− 0.0429	− 0.0047	0.0527
−8	0.6732	0.6756	0.6798	0.7336	0.4814
−7	0.0189	0.1608	0.1180	0.0072	− 0.0003
−6	− 0.6802	− 0.6716	− 0.6912	− 0.7085	− 0.5640
−5	0.0032	− 0.1588	− 0.1003	0.0024	0.0274
−4	**0.7140**	0.6122	0.7765	0.7373	0.4655
−3	0.0101	0.1682	0.1330	− 0.0059	0.0188
−2	− 0.7026	− 0.7639	− 0.6776	− 0.6980	− 0.5108
−1	0.0241	− 0.1581	− 0.0793	− 0.0108	0.0666
0	0.7464	0.7336	0.7890	0.7350	0.4345
1	0.0278	0.1641	0.1450	− 0.0002	0.0341
2	− 0.6801	− **0.7962**	− 0.6802	− 0.7203	− 0.4757
3	− 0.0166	− 0.1551	− 0.0979	− 0.0044	0.0695
4	0.6847	0.6726	**0.7927**	**0.7607**	**0.5271**
5	0.0109	0.1535	0.1258	− 0.0199	− 0.0047
6	− 0.6849	− 0.6901	− 0.6816	− 0.7023	− 0.5107
7	0.0381	− 0.1251	− 0.1000	− 0.0096	0.0235
8	0.7002	0.6572	0.6726	0.7299	0.4743
9	0.0312	0.1656	0.1488	0.0118	0.0487
10	− 0.6873	− 0.6308	− 0.6594	− 0.6777	− 0.4542

Note: Bold characters are the maximum values of SCCF (based on the absolute value).

Table 13 | Spearman cross-correlations (SCCF) between calculated monthly (1-month) RDI values in groups with stations with high spatial distance

	SCCF				
Lags	**Group 11**	**Group 12**	**Group 13**	**Group 14**	**Group 15**
−10	0.2855	0.3676	0.3086	0.3338	0.1834
−9	0.0483	0.1293	0.0630	− 0.0144	0.0312
−8	− 0.2492	− 0.1596	− 0.2090	− 0.3292	− 0.1890
−7	− 0.4985	− 0.4058	− 0.4493	− 0.5704	− 0.3062
−6	− 0.6202	− 0.5605	− **0.5517**	− 0.6471	− 0.3211
−5	− 0.5633	− 0.5398	− 0.4992	− 0.5186	− 0.2933
−4	− 0.2945	− 0.3763	− 0.2874	− 0.2696	− 0.1152
−3	0.0302	− 0.1133	− 0.0595	0.0305	0.0310
−2	0.3369	0.1722	0.2240	0.3179	0.1757
−1	0.5515	0.4158	0.4829	0.6399	0.3047
0	0.5838	0.5048	0.5176	0.6302	0.2887
1	0.4721	0.5639	0.5049	**0.7127**	**0.3766**
2	0.3088	0.3884	0.3173	0.3254	0.2121
3	0.0669	0.1400	0.0724	− 0.0050	− 0.0188
4	− 0.2201	− 0.1891	− 0.1966	− 0.3523	− 0.2005
5	− 0.4924	− 0.4182	− 0.4110	− 0.5645	− 0.3012
6	− **0.6273**	− **0.5788**	− 0.5316	− 0.6339	− 0.3304
7	− 0.5462	− 0.5453	− 0.4948	− 0.5247	− 0.2603
8	− 0.2933	− 0.3684	− 0.3058	− 0.2695	− 0.1226
9	0.0257	− 0.1401	− 0.0550	0.0171	0.0042
10	0.3038	0.1621	0.2228	0.3100	0.1785

Note: Bold characters are the maximum values of SCCF (based on the absolute value).

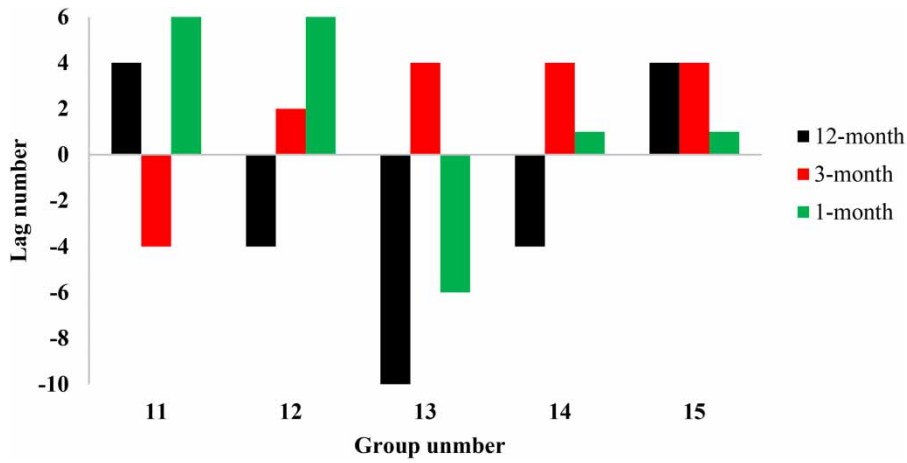

Figure 6 | The lag number with maximum value (based on the absolute value) of SCCF in calculated 1, 3, and 12-month RDI in groups with stations with high spatial distance.

analyzed. The results indicated that the proposed measure was more robust than the comparative measure, in detecting time delay between two non-Gaussian time series. The ability of the proposed measure in practice was also investigated by a real example. For this purpose, the RDI values of 20 synoptic stations in 1, 3, and 12-month time scales were considered and analyzed. The analysis results based on the actual data also proved the ability of the SCCF model. Finally, considering the low power of the CCF and high power of the SCCF to estimate CC in non-normal data series, it is suggested to assess the CC and calculate the time delay in non-normal hydrological data series the CCF replaced with the SCCF. On the other hand, it is recommended that SCCF's ability to determine the time delay in other hydrological variables such as rain and flood be investigated by other researchers.

ACKNOWLEDGEMENTS

The authors would like to thank National Meteorological Organization of Iran for providing the necessary climatic data.

AUTHORS CONTRIBUTION

The participation of M.R.M. and A.R.Z. includes the data collection, analyzing the results, and writing the article.

ETHICS APPROVAL

The authors confirm that this article is original research and has not been published or presented previously in any journal or conference in any language (in whole or in part).

DATA AVAILABILITY STATEMENT

Data cannot be made publicly available; readers should contact the corresponding author for details.

CONFLICT OF INTEREST

The authors declare there is no conflict.

REFERENCES

Abeysingha, N. S., Wickramasuriya, M. G. & Meegastenna, T. J. 2020 Assessment of meteorological and hydrological drought: a case study in Kirindi Oya river basin in Sri Lanka. *International Journal of Hydrology Science and Technology* **10** (5), 429–447.

Ablat, X., Liu, G., Liu, Q. & Huang, C. 2019 Application of Landsat derived indices and hydrological alteration matrices to quantify the response of floodplain wetlands to river hydrology in arid regions based on different dam operation strategies. *Science of the Total Environment* **688**, 1389–1404.

Aksoy, H., Cetin, M., Eris, E., Burgan, H. I., Cavus, Y., Yildirim, I. & Sivapalan, M. 2021 Critical drought intensity-duration-frequency curves based on total probability theorem-coupled frequency analysis. *Hydrological Sciences Journal* **66** (8), 1337–1358.

Aryal, Y. & Zhu, J. 2021 Spatial and temporal variability of drought patterns over the continental United States from observations and regional climate models. *Journal of Meteorological Research* **35** (2), 295–312.

Atif, I., Iqbal, J. & Mahboob, M. A. 2018 Investigating snow cover and hydrometeorological trends in contrasting hydrological regimes of the Upper Indus Basin. *Atmosphere* **9** (5), 162.

Bahrami, M., Bazrkar, S. & Zarei, A. R. 2021 Spatiotemporal investigation of drought pattern in Iran via statistical analysis and GIS technique. *Theoretical and Applied Climatology* **143** (3), 1113–1128.

Baik, J., Park, J., Hao, Y. & Choi, M. 2021 Integration of multiple drought indices using a triple collocation approach. *Stochastic Environmental Research and Risk Assessment* 1–19. https://doi.org/10.1007/s00477-021-02044-7.

Chen, J., Li, C., Brissette, F. P., Chen, H., Wang, M. & Essou, G. R. 2018 Impacts of correcting the inter-variable correlation of climate model outputs on hydrological modeling. *Journal of Hydrology* **560**, 326–341.

Dong, J., Wei, L., Chen, X., Duan, Z. & Lu, Y. 2020 An instrument variable-based algorithm for estimating cross-correlated hydrological remote sensing errors. *Journal of Hydrology* **581**, 124413.

El-Tantawi, A. M., Bao, A., Liu, Y. & Gamal, G. 2021 Assessment of meteorological drought in North-Western Egypt using rainfall deciles, standardized precipitation index and reconnaissance drought index. *Disaster Advances* **14**, 1–14.

Fang, B., Kansara, P., Dandridge, C. & Lakshmi, V. 2021 Drought monitoring using high spatial resolution soil moisture data over Australia in 2015–2019. *Journal of Hydrology* **594**, 125960.

Fattahi, M. H., Talebbeydokhti, N., Rakhshandehroo, G. R., Shamsai, A. & Nikooee, E. 2011 The robust fractal analysis of time series: concerning signal class and data length. *Fractals* **19** (01), 29–49.

Gumus, V., Simsek, O., Avsaroglu, Y. & Agun, B. 2021 Spatio-temporal trend analysis of drought in the GAP Region, Turkey. *Natural Hazards* 1–18. https://doi.org/10.1007/s11069-021-04897-1.

Han, Z., Huang, Q., Huang, S., Leng, G., Bai, Q., Liang, H., Wang, L., Zhao, J. & Fang, W. 2021 Spatial-temporal dynamics of agricultural drought in the Loess Plateau under a changing environment: characteristics and potential influencing factors. *Agricultural Water Management* **244**, 106540.

Han, M., Li, A., Gao, Z., Mu, D. & Liu, S. 2022 A survey of multi-class imbalanced data classification methods. *Journal of Intelligent & Fuzzy Systems*. (Preprint), 1-31. doi.10.3233/JIFS-221902.

Konapala, G., Kao, S. C. & Addor, N. 2020 Exploring hydrologic model process connectivity at the continental scale through an information theory approach. *Water Resources Research* **56** (10), e2020WR027340.

Kumar, U., Singh, S., Bisht, J. K. & Kant, L. 2021 Use of meteorological data for identification of agricultural drought in Kumaon region of Uttarakhand. *Journal of Earth System Science* **130** (3), 1–13.

Lashkari, A., Irannezhad, M., Zare, H. & Labzovskii, L. 2021 Assessing long-term spatio-temporal variability in humidity and drought in Iran using Pedj Drought Index (PDI). *Journal of Arid Environments* **185**, 104336.

Li, Q., He, P., He, Y., Han, X., Zeng, T., Lu, G. & Wang, H. 2020 Investigation to the relation between meteorological drought and hydrological drought in the upper Shaying River Basin using wavelet analysis. *Atmospheric Research* **234**, 104743.

Liang, J., Meng, Q., Li, X., Yuan, Y., Peng, Y., Li, X., Li, S., Zhu, Z. & Yan, M. 2021 The influence of hydrological variables, climatic variables and food availability on Anatidae in interconnected river-lake systems, the middle and lower reaches of the Yangtze River floodplain. *Science of the Total Environment* **768**, 144534.

Liu, H., Jia, J., Lin, Z., Wang, Z. & Gong, H. 2021 Relationship between net primary production and climate change in different vegetation zones based on EEMD detrending – a case study of Northwest China. *Ecological Indicators* **122**, 107276.

Lohpaisankrit, W. & Techamahasaranont, J. 2021 Analysis of precipitation and streamflow data for drought assessment in an unregulated watershed. *Environment and Natural Resources Journal* **19** (2), 112–121.

Lotfirad, M., Esmaeili-Gisavandani, H. & Adib, A. 2022 Drought monitoring and prediction using SPI, SPEI, and random forest model in various climates of Iran. *Journal of Water and Climate Change* **13** (2), 383–406.

Mahdavi, M. 2002 *Applied Hydrology*, Vol. 2. Tehran University Press, Tehran, p. 40.

Mallick, J., Talukdar, S., Alsubih, M., Salam, R., Ahmed, M., Kahla, N. B. & Shamimuzzaman, M. 2021 Analysing the trend of rainfall in Asir region of Saudi Arabia using the family of Mann-Kendall tests, innovative trend analysis, and detrended fluctuation analysis. *Theoretical and Applied Climatology* **143** (1), 823–841.

Mitková, V. B. 2019 Effect of the data length and seasonality on the accuracy of T-year discharges estimation: case study on the Topľa River. *Acta Hydrologica Slovaca* **20** (2), 113–121.

Mohammed, Y. & Yimam, A. 2021 Analysis of meteorological droughts in the Lake's Region of Ethiopian Rift Valley using reconnaissance drought index (RDI). *Geoenvironmental Disasters* **8** (1), 1–16.

Mokarram, M. & Zarei, A. R. 2021 Determining prone areas to gully erosion and the impact of land use change on it by using multiple-criteria decision-making algorithm in arid and semi-arid regions. *Geoderma* **403**, 115379.

Myronidis, D., Ioannou, K., Fotakis, D. & Dörflinger, G. 2018 Streamflow and hydrological drought trend analysis and forecasting in Cyprus. *Water Resources Management* **32** (5), 1759–1776.

Peña-Gallardo, M., Vicente-Serrano, S. M., Hannaford, J., Lorenzo-Lacruz, J., Svoboda, M., Domínguez-Castro, F., Maneta, M., Tomas-Burguera, M. & El Kenawy, A. 2019 Complex influences of meteorological drought time-scales on hydrological droughts in natural basins of the contiguous United States. *Journal of Hydrology* **568**, 611–625.

Piri, H. & Mobaraki, M. 2021 Comparison of rainfall and evapotranspiration-based drought indices to determine meteorological drought. *Environment and Water Engineering* **7** (2), 328–343.

Radmanesh, F., Esmaeili-Gisavandani, H. & Lotfirad, M. 2022 Climate change impacts on the shrinkage of Lake Urmia. *Journal of Water and Climate Change*. https://doi.org/10.2166/wcc.2022.300

Rahmani, F. & Fattahi, M. H. 2021 A multifractal cross-correlation investigation into sensitivity and dependence of meteorological and hydrological droughts on precipitation and temperature. *Natural Hazards* 1–23. https://doi.org/10.1007/s11069-021-04916-1.

Roustaei, F., Ebrahimi Khusfi, Z., Kousari, M. & Mokhtari, M. 2021 Investigating lagged cross-correlation between wind erosion and drought in Southern Iran's arid regions. *Desert Ecosystem Engineering Journal* **3** (2), 29–42.

Sadatinejad, S. J., Hassanshahi, R., Shayannejad, M. & Abdolahi, K. 2011 Evaluation of Fuzzy regression efficiency for reconstructing missing annual precipitation data in Karoon basin. *Environmental Science* **8** (3), 109–116.

Salimi, H., Asadi, E. & Darbandi, S. 2021 Meteorological and hydrological drought monitoring using several drought indices. *Applied Water Science* **11** (2), 1–10.

Seo, S. B., Bhowmik, R. D., Sankarasubramanian, A., Mahinthakumar, G. & Kumar, M. 2019 The role of cross-correlation between precipitation and temperature in basin-scale simulations of hydrologic variables. *Journal of Hydrology* **570**, 304–314.

Sun, P., Ma, Z., Zhang, Q., Singh, V. P. & Xu, C. Y. 2022 Modified drought severity index: model improvement and its application in drought monitoring in China. *Journal of Hydrology* **612**, 128097.

Tai, X., Anderegg, W. R., Blanken, P. D., Burns, S. P., Christensen, L. & Brooks, P. D. 2020 Hillslope hydrology influences the spatial and temporal patterns of remotely sensed ecosystem productivity. *Water Resources Research* **56** (11), e2020WR027630.

Tsakiris, G. 2004 Meteorological drought assessment. Paper Prepared for the Needs of the European Research Program MEDROPLAN (Mediterranean Drought Preparedness and Mitigation Planning), Zaragoza, Spain.

Tsakiris, G., Pangalou, D. & Vangelis, H. 2007 Regional drought assessment based on the Reconnaissance Drought Index (RDI). *Water Resources Management* **21** (5), 821–833.

Tuan, N. H. & Canh, T. T. 2021 Analysis of trends in drought with the non-parametric approach in Vietnam: a case study in Ninh Thuan Province. *American Journal of Climate Change* **10** (01), 51.

Zarei, A. R. & Mahmoudi, M. R. 2021 Assessing the influence of PET calculation method on the characteristics of UNEP aridity index under different climatic conditions throughout Iran. *Pure and Applied Geophysics* 1–27. https://doi.org/10.1007/s00024-021-02786-z.

Zarei, A. R. & Moghimi, M. M. 2019 Environmental assessment of semi-humid and humid regions based on modeling and forecasting of changes in monthly temperature. *International Journal of Environmental Science and Technology* **16**, 1457–1470.

Zarei, A. R., Shabani, A. & Mahmoudi, M. R. 2020 Evaluation of the influence of occurrence time of drought on the annual yield of rain-fed winter wheat using backward multiple generalized estimation equation. *Water Resources Management* **34** (9), 2911–2931.

Zarei, A. R., Shabani, A. & Moghimi, M. M. 2021a Accuracy assessment of the SPEI, RDI and SPI drought indices in regions of Iran with different climate conditions. *Pure and Applied Geophysics* **178** (4), 1387–1403.

Zarei, A. R., Shabani, A. & Mahmoudi, M. R. 2021b Susceptibility assessment of winter wheat, barley and rapeseed to drought using generalized estimating equations and cross-correlation function. *Environmental Processes* **8** (1), 163–197.

Zarei, A. R., Moghimi, M. M. & Koohi, E. 2021c Sensitivity assessment to the occurrence of different types of droughts using GIS and AHP techniques. *Water Resources Management.* **35**, 3593–3615.

Zarei, A. R., Mahmoudi, M. R. & Moghimi, M. M. 2022 Determining the most appropriate drought index using the random forest algorithm with an emphasis on agricultural drought. *Natural Hazards* 1–24. https://doi.org/10.1007/s11069-022-05579-2.

Zhang, Y., Hao, Z., Feng, S., Zhang, X., Xu, Y. & Hao, F. 2021 Agricultural drought prediction in China based on drought propagation and large-scale drivers. *Agricultural Water Management* **255**, 107028.

First received 3 September 2022; accepted in revised form 6 January 2023. Available online 19 January 2023